CHALMERS

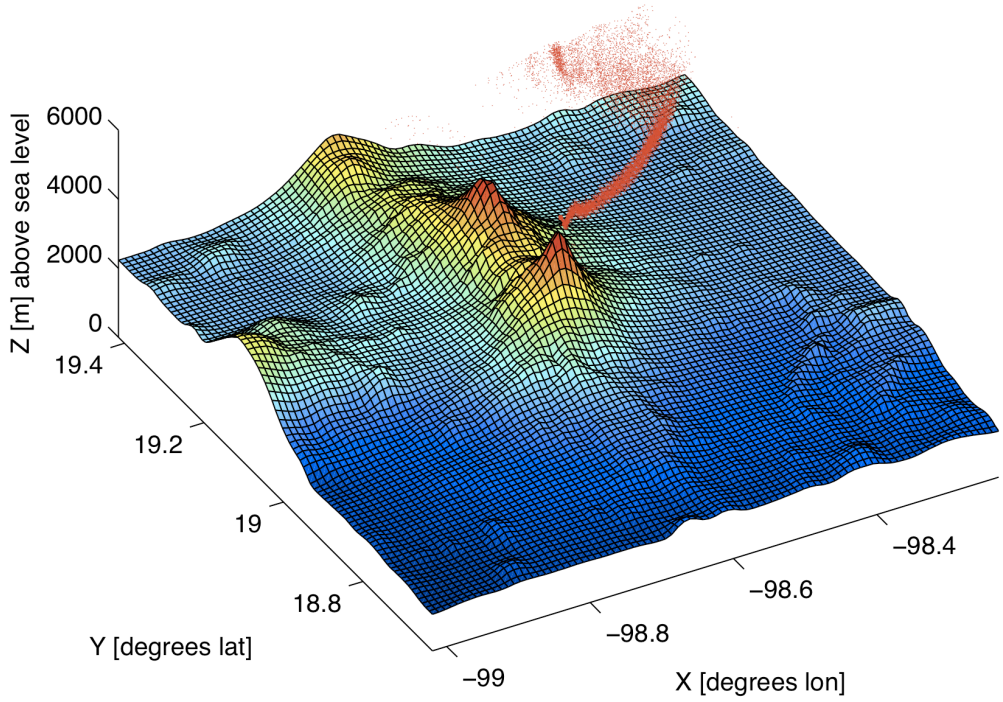

Implementation and Validation of a Meteorological Dispersion Model Applied on Volcanic Gas Emission for Studies of Environmental Impact

Master of Science Thesis

OSKAR LANDGREN

Department of Earth and Space Science
Optical Remote Sensing Group
CHALMERS UNIVERSITY OF TECHNOLOGY
Gothenburg, Sweden, 2011

Implementation and Validation of a Meteorological Dispersion Model Applied on Volcanic Gas Emission for Studies of Environmental Impact

OSKAR LANDGREN

Department of Earth and Space Science
Optical Remote Sensing Group
CHALMERS UNIVERSITY OF TECHNOLOGY
Gothenburg, Sweden, 2011

Implementation and Validation of a Meteorological Dispersion Model Applied on Volcanic Gas Emission for Studies of Environmental Impact
OSKAR LANDGREN

Department of Earth and Space Science
Chalmers University of Technology
SE-412 96 Göteborg
Sweden
Telephone + 46 (0)31-772 1000

Cover:
The simulated plume from FLEXPART-WRF at 2010-04-22 22:00 UTC for the volcano Popocatépetl.

Department of Earth and Space Science
Göteborg, Sweden 2011

Implementation and Validation of a Meteorological Dispersion Model Applied on Volcanic Gas Emission for Studies of Environmental Impact

OSKAR LANDGREN
Department of Earth and Space Science
Chalmers University of Technology

ABSTRACT
The Lagrangian atmospheric transport model FLEXPART-WRF was implemented to model dispersion of volcanic gas emitted from the three volcanoes Popocatépetl in Mexico (lat: 19.02, lon: -98.62), Tungurahua in Ecuador (lat: -1.47, lon: -78.44) and Nyiragongo in D.R. Congo (lat: -1.52, lon: 29.25). Meteorological data from ECMWF with 1/8th degree spatial resolution and 6 hour temporal resolution was fed into the mesoscale meteorological model WRF (Advanced Research WRF 3.2.1) and run for three nested grids with 9, 3 and 1 km resolution with hourly outputs. This data was provided into FLEXPART-WRF, simulating emissions of 100 000 particles per day. The modelled concentration fields were used for producing sum of concentrations in slant and vertical columns which were compared to measurement data from scanning differential optical absorption spectroscopy (DOAS) instruments between 5 and 15 km from the volcanoes as well as car traverse measurements using mobile DOAS instruments. The model shows agreement with individual scans from the scanning instruments but the spread in the results of quantifiable parameters such as plume height and width is large. When comparing with the mobile measurements the model gives very good agreement in about two thirds of the cases. Finally, a simulation of ground dose over one month (December 2009) was also performed for Nyiragongo.

Keywords: dispersion modelling, atmospheric transport, volcanic gas emission, SO2, FLEXPART

Contents

Preface and acknowledgement

This master's thesis work was carried out during autumn 2010 and spring 2011 and preceded by a field campaign on Popocatépetl volcano in Mexico (Long: -98.63°, Lat: 19.02°) as a means of data collection and familiarising with the instruments used in the measurement process.

It was supported by an introductory course in meteorology at Uppsala University in September-October during which time collaboration was started between our two departments in Uppsala University and Chalmers. From that time I would like to thank Magnus Baltscheffsky and his supervisor Anna Rutgersson Owenius (PhD, Associate Prof.[1]) for meteorological advice and support.

Throughout the whole period I am very grateful and would like to thank the PhD students in our Optical Remote Sensing group[2], Santiago Arellano and Vladimir Conde for their thorough knowledge about the instrumentation and measurements and especially Patrik Norman for providing meteorological model data and countless hours of advice regarding the method and implementation.

I would also like to thank Jerome D. Fast at PNNL for letting us use his further development of FLEXPART-WRF, PILT.

Last but not least I would like to thank my supervisor Bo Galle (PhD, Associate Prof.[2]), who despite a constantly heavy workload always has given me encouraging support.

[1]Dept. of Earth Sciences, Uppsala University
[2]Dept. of Earth and Space Sciences, Chalmers University of Technology, Gothenburg

Notations

Table 1: A collection of annotations used in this thesis.

AGL	Above Ground-Level
ASL	Above Sea-Level
Cospec	Correlation Spectrometer
DOAS	Differential Optical Absorption Spectroscopy
DORSIVA	Development of Optical Remote Sensing Instruments for Volcanological Applications
NOVAC	Network for Observation of Volcanic and Atmospheric Change
ORS	Optical Remote Sensing
PILT	PNNL Integrated Lagrangian Transport
VEI	Volcanic Explosivity Index
WRF	Weather Research and Forecasting model

1 Introduction

Historically, numerical approximation of pollution dispersion have been used to model transport of emissions from localised sources, e.g. from industrial chimneys or in the event of a nuclear disaster. One of the earliest articles on numerical approximations of dispersion of pollutant from an industrial chimney was published in 1936, [5]. The advent of computers led to the development of a number of different numerical models in the 1960's. Nowadays dispersion modelling has found widespread uses in estimating the local, regional and global impact of both man-made (e.g. vehicular traffic, industries) as well as natural (wildfires, volcanoes) emission sources.

1.1 Background

Volcanoes all over the world continuously emit large volumes of different gases and particles and is the most abundant natural source of atmospheric SO_2. These gases in turn have impact on the environment both locally and globally. Volcanic particles (and sulphuric salts formed by oxidation of SO_2) act as condensation nuclei and influence cloud formation processes, affecting the microclimate as well as partially counteracting global warming.

We have been reminded numerous times, recently by the eruption of the two Icelandic volcanoes Grímsvötn in May 2011 and Eyafjallajökull in April 2010, that volcanoes can halt important functions in society. There is no doubt need for accurate simulations of dispersion of volcanic gas and particles.

Since the Optical Remote Sensing (ORS) group at Chalmers has access to a large network of stations measuring volcanic SO_2 the measurements can be used to to validate modelled dispersion.

The Optical Remote Sensing group at the Department of Earth and Space Science has over the last 10 years coordinated two EU research projects related to volcanic gas emission measurements. In the first project, DORSIVA (Development of Optical Remote Sensing Instruments for Volcanological Applications), which ran from Oct 2002 to Sept 2005, different instrumentation methods were developed to address the issue of measuring volcanic gas emissions. The second project, NOVAC, Network for Observation of Volcanic and Atmospheric Change, applied the knowledge from DORSIVA by constructing a network of stations with stations monitoring the emissions of gases from a selection of volcanoes all over the world. The group is also presently running a SIDA project related to gas emissions from the volcano Nyiragongo in the Democratic Republic of Congo.

1.1.1 NOVAC

The Network for Observation of Volcanic and Atmospheric Change (NOVAC) is a network of automatic ground-based measurement stations utilising Differential Optical Absorption Spectroscopy (DOAS) instruments in the UV region to measure gas emissions from volcanoes. The data is used primarily for volcanic risk assessment but also for geophysical research, studies of atmospheric change and ground validation of satellite measurement. The project was funded by the European Union during the years 2004-2010. Currently the network contains 59 instruments continuously measuring the emissions of SO_2 from 19 volcanoes in 13 countries on five continents. The map of covered volcanoes for 2009 is shown in fig. 1. Most of the

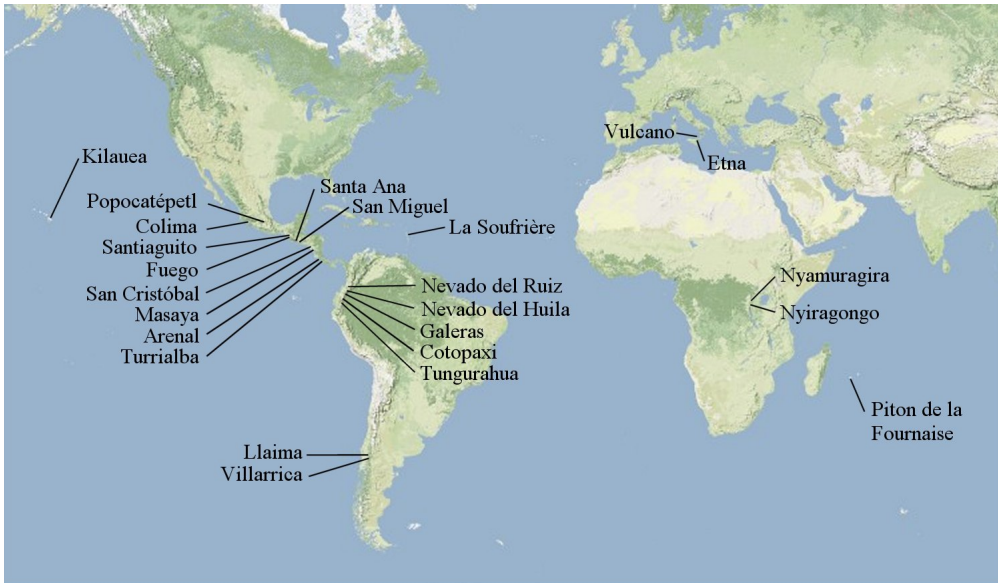

Figure 1: Map showing the NOVAC instruments as of 2009. Since then instruments have also been installed on Iceland and the Philippines. Map from [1].

volcanoes are located in Latin America, but there are also instruments on volcanoes in Italy, Iceland, Reunion island, D.R. Congo as well the Philippines. Some are among the most active and strongly degassing volcanoes in the world. The large dataset has both long time series and high time resolution and gives a unique opportunity for research.

1.1.2 SIDA Congo project

The ongoing project 'Studies of the gas emissions from Nyiragongo volcano, Democratic Republic of Congo, with respect to volcano risk assessment and environmental impact' is funded by SIDA and run by Chalmers and Uppsala University. The project builds upon foundations laid by several other projects: a UN-OCHA (Office for the Coordination of Humanitarian Affairs) project 'SO_2 flux monitoring system for Nyiragongo', the EU project NOVAC mentioned above, a Belgium/Luxembourg/Italy multidisciplinary project GORISK related to risk mitigation and assessment, as well as another SIDA project 'Studies of the environmental impact of gases from Nyiragongo volcano, Democratic Republic of Congo' (SWE-2008-064) which acted as the first phase of this project.

This master thesis goes partly into one of the objectives of the project, which is to implement a plume dispersion model for Nyiragongo. The model will then be run using meteorological data for a year to produce statistical maps of likely average SO_2 concentrations downwind from the volcano and provide this data to the GORISK project to support epidemiological studies. The objectives following the implementation of the dispersion model also includes validation of the dispersion model by more measurements (DOAS and FTIR) as well as placement of passive chemical samplers on the ground.

1.2 Volcano sites

This study used measurement data from three volcanoes: Popocatépetl (lat. 19.02°, lon. -98.63°) in Mexico, Tungurahua (lat: -1.47°, lon: -78.44°) in Ecuador and Nyiragongo (lat. -1.52°, lon. 29.25°) in D.R. Congo.

1.2.1 Popocatépetl

Popocatépetl is a stratovolcano located about 70 km southeast of Mexico City (see fig. 2), where the borders of the states Mexico, Morelos and Puebla meet. With its peak at 5426 m, it is the second highest peak in Mexico, after another volcano, Pico de Orizaba.

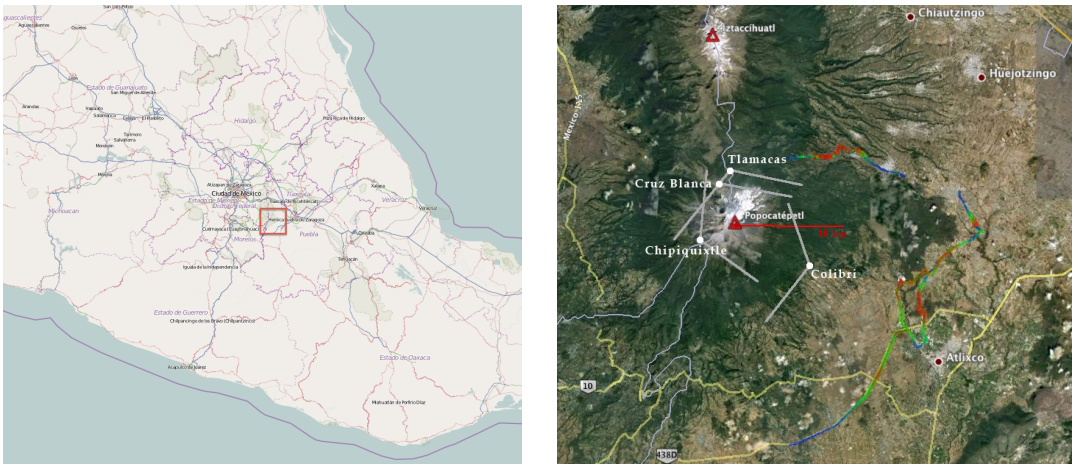

Figure 2: Map of Popocatépetl and its surroundings. The red square in the left map is enlarged to the right. The four white dots encircling the volcano are the NOVAC instruments with their outer scanning angles shown as grey lines. A selection of car traverse measurements are shown as the colored lines to the south-east. The red line of 10 km length is included as scale.

Popocatépetl, which means 'Smoking Mountain' in Nahuatl, has ongoing eruptions with a volcanic explosivity index of 2 and emits gas continuously. Its latest big eruption took place in December 2000, with lava and pyroclastic flows and lahars (mudflows).[2] 56 000 people were evacuated from 40 villages within 12 km from the crater.

The SO_2 emissions from Popocatépetl amount to between 100 and 8 000 tonnes per day[3] and is monitored by the agency CENAPRED (National Center for Prevention of Disasters) operating measuring stations around the volcano with various instruments, including 4 scanning NOVAC instruments. The safe and relatively accessible roads makes it a good candidate for measurement campaigns.

Figure 3: View of Popocatépetl from Paso de Cortes just north of the volcano. The hill to the left with the masts is an historical lava dome where the Tlamacas station is located.

1.2.2 Tungurahua

Tungurahua is a stratovolcano located in Ecuador, about 140 km south of the capital Quito. Its name means 'Throat of Fire' in Quichua. With no major eruption since 1916, the volcano in October 1999 begun an eruptive period which is still ongoing with continuous gas emission as of today. The prevailing wind direction of the site is easterly, blowing the plume to the west of the crater, with compass direction between 230° and 290° from the volcano 90% of the time, and plume height above sea level between 4000 and 5700 m.[1]

Three NOVAC instruments were installed in 2007 in locations to the west of the volcano, giving excellent cover of the mentioned range, while also providing frequent triangulation measurements of plume height.

1.2.3 Nyiragongo

Mt Nyiragongo is located in Nord-Kivu, in the eastern part of the Democratic Republic of the Congo, about 40 kilometers from the intersection of the borders of Congo, Rwanda and Uganda and 20 kilometres north of Lake Kivu. Nyiragongo is a part of a series of volcanoes along the Great Rift Valley which is formed between the two African tectonic plates. Its closest neighbouring volcano Nyamuragira is Africa's most active volcano with over 40 eruptions since the late 19th century. About 2 million people live in the area around Lake Kivu, of which around half a million in the city of Goma, stretching from the shore and down to just 13 km from the crater. The low silica contents of the lava makes it flow very easily and due to the steep slopes of the stratovolcano its speed can be up to 100 km/h.

Nyiragongo emits between 2 000 and 50 000 metric tonnes of SO_2 per day. (Compare with e.g. total emissions of SO_x in Sweden of about 83 000 tonnes per day in 2008. [4]) In addition to the risks associated with eruptions, the gases emitted from the two volcanoes cause severe health problems to the local inhabitants. People are collecting and drinking the rainwater and since rain forms where particles are present for condensation, e.g. in the volcanic plume, even dental loss is common due to high concentrations of acidic HF.

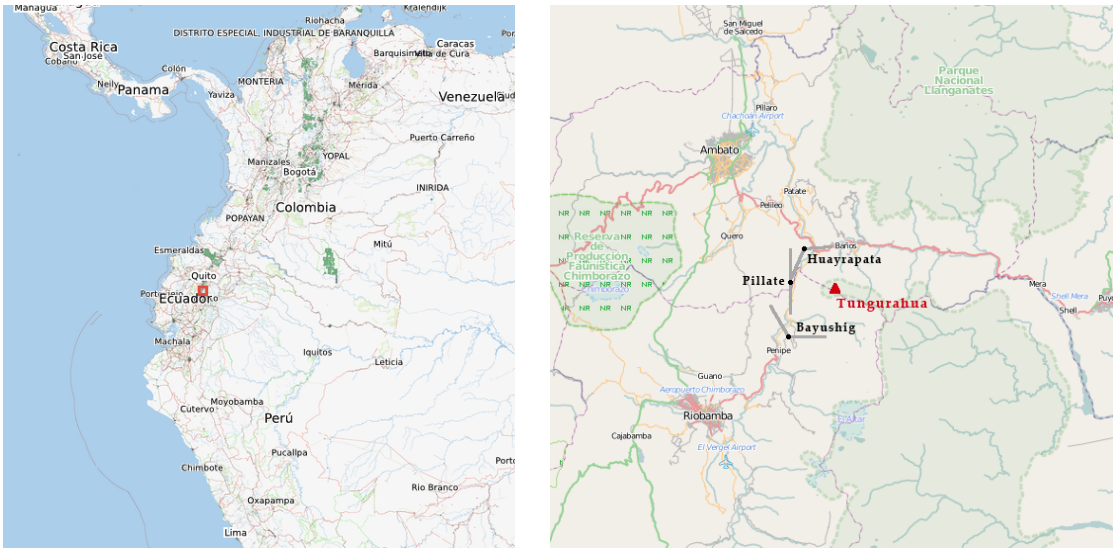

Figure 4: Map of Tungurahua and its surroundings. The red square in the left map is enlarged to the right. The three black dots in the right map are the NOVAC stations with their outer scanning angles shown as grey lines. Both maps ©Openstreetmap & contributors.

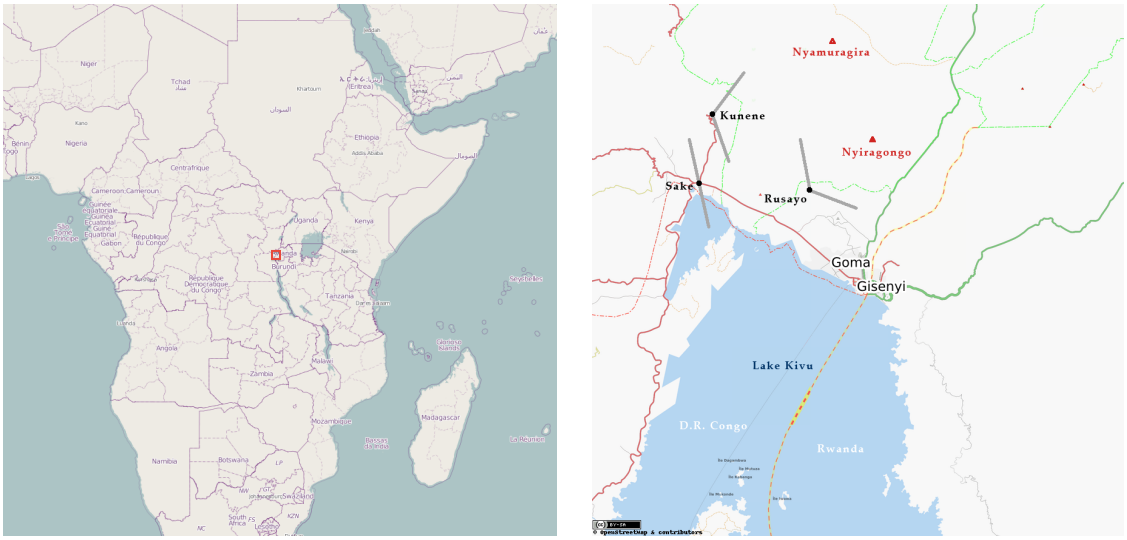

Figure 5: Map of Nyiragongo and its surroundings. The red square in the left map is the enlarged to the right. The three black dots in the right map are the NOVAC stations with their outer scanning angles shown as grey lines. Both maps ©Openstreetmap & contributors.

In 2004 the first scanning DOAS instrument was installed in the area with support from UN-OCHA. In 2007 the existing instrument was upgraded and complemented with an additional 3 instruments as part of the EU project NOVAC.

In 2012 a campaign will take place on Nyiragongo. Several passive chemical diffusion samplers will be placed to measure cumulative ground concentration of SO_2.

1.3 Aim and objectives

- To implement an atmospheric dispersion model on the volcanoes Popocatépetl (Mexico), Tungurahua (Ecuador) and Nyiragongo (D.R. Congo) using data from the mesoscale meteorological model WRF.
- To validate the model using optical remote sensing data from Popocatépetl and Tungurahua.
- To process simulation data for a year at Nyiragongo and make average values of ground concentration levels of SO_2.

1.4 Delimitations

There are numerous other numerical dispersion models available (e.g. CALPUFF, EMEP, FLEXPART, HYSPLIT). FLEXPART-WRF was chosen mainly due to the amount of high-resolution WRF data at hand used in wind and flux measurements. Efforts to compare with other models are not made in this project.

2 Theory

Since a gas consists of a very large number of molecules, dispersion can never be modelled on an individual molecular level. Different approximations can be made in order to make the modelling easier. Some quantities can be described by macro scale field quantities which can then be related using model equations, giving for example a concentration field instead of individual molecules. On a smaller scale, it is possible to consider small particles or air parcels instead of fields.

2.1 Diffusion of gases

For a concentration field $\phi = f(x, y, z, t)$, Fick's first law of diffusion states that the flux J of a substance through unit area per unit time is proportional to the spatial gradient of the concentration.

$$J = -D\nabla\phi \tag{1}$$

The proportionality constant D is called diffusion constant, which is compound specific with unit area per time. The change in concentration is described by Fick's second law of diffusion, which is a analogous to the heat equation.

$$\frac{\partial\phi}{\partial t} = \nabla^2 D\phi \tag{2}$$

The equations above can also be applied to particles, using the Stokes-Einstein equation

$$D = kT\mu = kTv_d/F = \frac{kTC_c}{3\pi\eta d}$$

where k is the Boltzmann constant, T is absolute temperature, μ is the mobility, v_d is the terminal drag velocity, d is the diameter of the particle and C_c is the Cunningham slip correction factor.

For lab environments, these diffusion equations can sometimes give a sufficient description of the behaviour, but usually the effects from diffusion are not as important for dispersion as another phenomenon, turbulence.

2.2 Turbulence

Turbulent motion is the main phenomenon governing atmospheric transport of concentration gradients. It occurs when these gradients are steep enough in combination with presence of density gradients (e.g. from temperature gradients) and high flow velocities (to overcome the inertial forces). Due to their random and chaotic nature, turbulent flows have no deterministic exact solutions and so they are always modelled statistically.

In order to explain turbulence some characteristic parameters are often used. The wind speed v can be written as $v = \bar{v} + v'$, where $\bar{v}$ is the average wind speed and v' is the fluctuating part.

Turbulent flows incorporate a lot of different length scales, where the smallest can be calculated using the Kolmogorov length scale, $\eta = (\nu^3/\epsilon)^{1/4}$, where ν is the kinematic viscosity and ϵ is the energy dissipation per mass. Similar relations exist for the time and velocity scales. (Also note that the kinematic viscosity may also be written as $\nu = \mu/\rho$, where μ is the dynamic viscosity and ρ is the density.)

The energy associated with the whole system can be given in terms of the turbulence kinetic energy, which is the mean of the squared velocity fluctuations per unit mass, i.e. $\text{TKE} = \frac{1}{2}\overline{(v')^2}$. It is an important variable for meteorology in the boundary layer and directly relates to the transport of momentum, heat and moisture. Naturally, more energy in the turbulent system means more mixing. Using Kolmogorov's theory (1941), with C being a constant, TKE can also be written as

$$\text{TKE} = \int_0^\infty C\epsilon^{2/3}(2\pi/r)^{-5/3}$$

Two important ratios often used in turbulence are the Reynolds number, *Re*, and the Richardson number, *Ri*. The first is the ratio between the inertial and viscous forces acting on a fluid,

$$\text{Re} = \frac{\text{drag force}}{\text{viscous force}} = \frac{\rho V^2 L^2}{\mu V L} = \frac{\rho V L}{\mu} = \frac{V L}{\nu}$$

where V is the (local) velocity relative to the fluid and L is a characteristic length scale of the system. For a high Re value (usually in the order of thousands), i.e. where the inertial forces (drag) dominate, the flow is *turbulent* and produces eddies and vortices and the mixing is more random. When the Re value is lower the flow is called *laminar* and the mixing is much less effective.

In a similar way, the Richardson number is the ratio of potential and kinetic energy, $\text{Ri} = gh/v^2$, where g is the gravitational acceleration and h and v are characteristic lengths and velocities. In the free atmosphere the Richardson number is usually between 0.1 and 10, with values below 1 meaning significant turbulence.

The transition between turbulent and laminar flow can be put in terms of Reynolds or Richardson numbers and is also dependent on the geometry of the

fluid situation, i.e. obstacles and turns as well as the width of the flow channel. For many theoretical cases such as flow in tubes, with cross-sections of simple geometrical shapes, simple theoretical solutions exist that agree well with observations.

On a scale which is large enough to not consider the microstructure like single eddies and vortices but small enough to not let the net flow direction matter, the random motion in turbulent diffusion results in a normal (Gaussian) distribution.

2.3 Dispersion modelling

Approaching smaller scale, we may consider a solid spherical particle with a fixed size and mass. Forces acting on the particle (including e.g. contact, drag and electrostatic forces) will cause the particle to accelerate and change direction. A model operating on particles is however not only useful for particular emissions such as volcanic ash, radionuclides from a nuclear accident or soot particles from an ordinary industrial chimney. In meteorology and atmospheric physics, one often talk about air parcels, which are like isolated masses of gas which are in thermodynamic equilibrium with their surroundings. As they rise they undergo (adiabatic) expansion as the pressure drops, but the mass within the parcel remains constant.

In the 1936 article [5], Bosanquet et al. assumed a normal distribution of the gas emitted from a chimney. Models based on this are called **Gaussian models**. An example of the equation for the concentration field C (from [6]), along the wind direction, is

$$C(x,y,z) = \frac{Q}{u} \cdot \frac{e^{-y^2/2\sigma_y(x)^2}}{\sigma_y(x)\sqrt{2\pi}} \cdot \frac{g(z)}{\sigma_z(x)\sqrt{2\pi}} \tag{3}$$

where Q is the source emission rate [mass/time], u is the horizontal wind velocity along the plume centre line, σ is a dispersion coefficient, corresponding to the standard deviation in the normal distribution of gas concentration spatially in the respective dimensions. σ_x and σ_y are functions of the distance from the source point, e.g. $\sigma_y(x) = c_1 x^{c_2}$ and $\sigma_z(x) = c_3 x^{c_4} + c_5$. The values of c_n are tabulated and change depending on the turbulence, often simplified as the Pasquill atmospheric stability classes, which in turn depend on the surface wind speed and the incoming solar radiation (for more information see e.g. [7]). The vertical dispersion parameter g is different for accounting for different reflections (none, from the ground and/or inversion layer above). If the emission is not continuous, a 'puff' approach can be used, i.e. the plume is seen as a number of different releases at different times, which can be modelled as individual plumes each with their own Gaussian dispersion.

In **box models** a fixed grid is used in which the variables (input data such as winds, temperature etc. as well as output data, e.g. particle concentration) are calculated for each grid box. The concentration in the boxes influence each adjacent box by mass diffusion between each time step. The main advantage is computational efficiency and easy data handling since the fields can be stored in large 4D-matrices. However, a very spatially localised emission will instantly be mixed within the enclosing grid box (a phenomenon known as numerical diffusion) and the accuracy and model run time depends strongly on grid size. Box models are therefore not as computationally efficient as many other models.

Another approach is to insert a tracer particle into the model at the release position. The particle is then followed, with its motion depending on the meteorological data. These **Lagrangian models** use a coordinate system which follows the particle (or air parcel) of interest. The position of each particle is given as the vector from a common reference point so there is no limit in resolution as in box models.

By placing a larger number of tracer particles in a four-dimensional box (x,y,z,t) around the release location and following them all, an approximation of the plume dispersion is given. The more particles used the better they resemble the plume. After completing a run with a Lagrangian model, the concentration can still be calculated in a grid for easier handling.

A disadvantage with tracers is that a lot of small particles will not improve the results closer to the plume but those particles still require computation time. This can be improved by for example splitting the parcels after a certain time, giving a fraction of the original mass to each new parcel. In a real-life situation attention also has to paid to water vapour since the energy released upon condensation (latent heat) is substantial. If this is ignored the case is called dry adiabatic.

2.4 Particle motion and trajectories

A particle trajectory is the spatial path taken over time by a moving particle (or air parcel). Trajectories can be either forward, e.g. for forecasting when and where an emission will be transported, or backward, retracing the possible sources of an observed local concentration. An example of a forward trajectory for Popocatépetl is shown in fig. 6. Plots can similarly be made by following test particles from different emission altitudes to show the significance of chimney altitude etc.

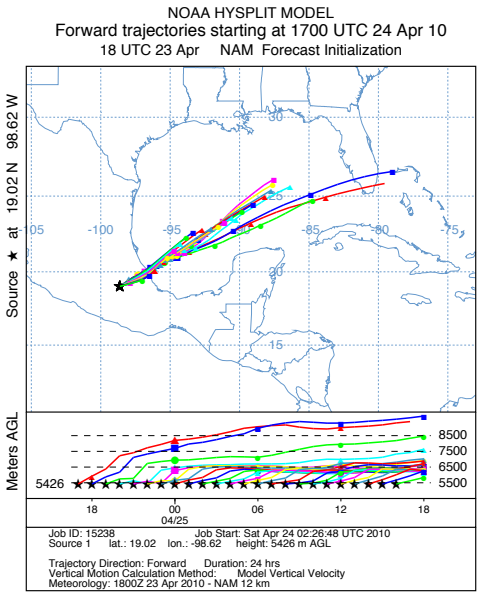

Figure 6: An example trajectory simulated for particles emitted from Popocatépetl on 2010-04-24 at 17:00 UTC, modelled by HYSPLIT using meteorological forecast data from NAM. Different release times can be followed on the map, with their altitudes plotted below.

2.5 Models

In short, the workflow for atmospheric dispersion modelling consists of using meteorological data together with data on topography, time evolution and spatial information of the release characteristics, applying numerical equations approximating the physical behaviour of the released substance in the atmosphere.

Since the typical distance from the measurement instruments to the crater are on the order of 5-15 kilometres and since volcanoes constitute local topographic variations of several kilometres in height, none of the global meteorological model datasets ECMWF ($0.125° \approx 14$ km resolution, every 6 hours) or GFS ($1° \approx 110$ km res., every 6 hours) could be used directly. Instead this global data was fed into the mesoscale meteorological model WRF to increase the resolution and pay attention to the local topography. The model FLEXPART-WRF/PILT, based on FLEXPART was chosen as dispersion model. Even though this model is based on an older version of FLEXPART (6.2, current 8.2) it was considered better suited for this short-range transport scenario.

The actual workflow used is summarised in fig. 7. This section contains a brief summary of the models used in this work.

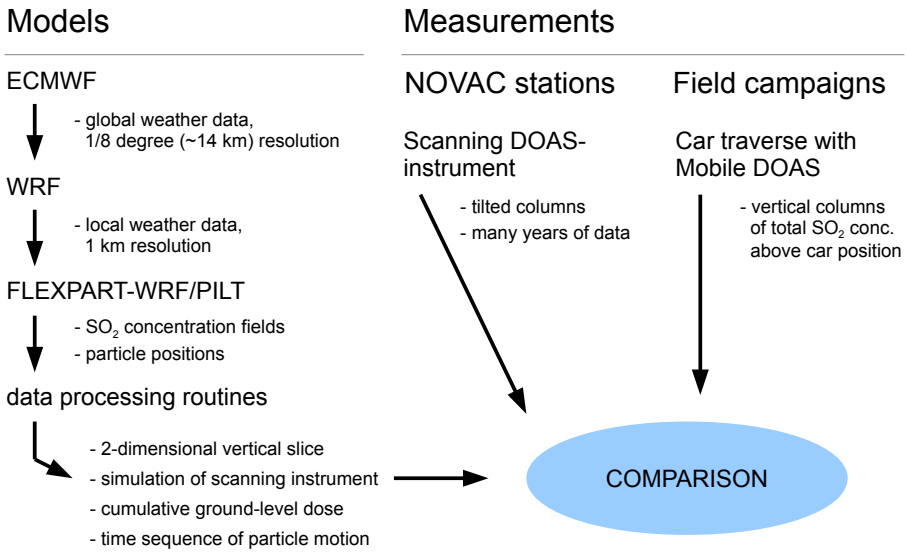

Figure 7: Workflow. Models are fed with data in the sequence shown, producing output data which is then compared with measurement data from stationary and mobile instruments.

2.5.1 ECMWF

European Centre for Medium range Weather Forecast assimilates huge number of synoptic observations from both weather stations, meteorological balloons and satellites and feed them into a global model which is run continuously on their compute cluster. The model is both run in forecast mode and produces re-analysis of older data.[8]

The ECMWF model uses a spectral approach, which means that instead of parameterising the meteorological fields on a grid with fixed resolution, they are represented

by a series of harmonic functions by Fourier transform. Solutions to meteorological equations involving partial derivatives are then easily determined exactly and then output to a grid for convenience when feeding into other models. The resolution of the model is determined by the highest frequency component (shortest wavelength) in the waves. A spectral approach is very suitable for global models since the spherical geometry implies that the modelled weather must have a 360° (longitude and latitude) periodicity.

In this work the data from the ECMWF model is used as input for the mesoscale meteorological model WRF.

2.5.2 WRF

The Weather Research and Forecasting model [9] or WRF, pronounced [warf], is a non-hydrostatic mesoscale numerical meteorological model. Mesoscale means that the model operates between 1 and 1000 km, and so it does not consider phenomenon on micro-scale or synoptic scale.

WRF utilises nested grids within each other with different resolutions to get better predictions in the area of interest while still keeping enough data for the surroundings.

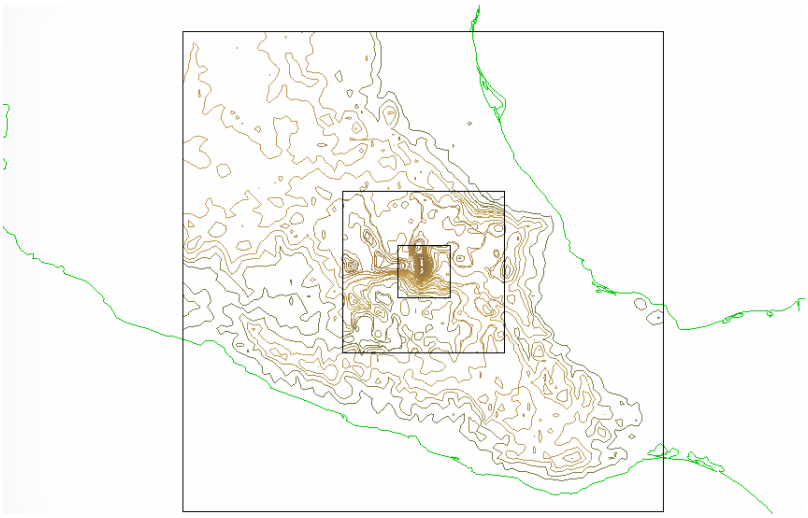

Figure 8: Nested model domains over the volcano Popocatépetl in Mexico. The grids are 91 points in both longitude and latitude direction, with a resolution of about 9, 3, and 1 km respectively.

2.5.3 FLEXPART

FLEXPART is a Lagrangian particle dispersion model. It is capable of backward and forward trajectory simulations of particles (or infinitely small air parcels) released from point, line or volume sources. Different versions of the model enables use of input data from global numerical weather prediction models from ECMWF, NOAA (GFS) as well as mesoscale models (MM5, WRF, COSMO). Removal processes incorporated into the model include radioactive decay, dry and wet deposition and OH reaction. A technical note describing the model is available [10].

FLEXPART was written by Andreas Stohl (currently at NILU, Norway) during his military service at the nuclear-biological-chemical school of the Austrian Forces. Since then it has seen numerous updates and incorporated improvements from multiple authors.

The latest version of FLEXPART (as of May 2011) is 8.2. This version uses weather data from either GFS or ECMWF. From version 6.2 an additional branch, FLEXPART-WRF, has been developed by Jerome D. Fast of Pacific Northwest National Laboratory. This version enables the use of output from the WRF model instead of ECMWF or GFS. The new version is called PILT.

2.5.4 PILT

The PNNL Integrated Lagrangian Transport (PILT) model is based on FLEXPART 6.2 but has been extensively changed by Jerome D. Fast, Richard C. Easter and Weiguo Wang at Pacific Northwest National Laboratory 2006-2007, [11], [12] and [13]. It is integrated both in the sense that it takes GFS as well as WRF data, and that it handles both backward and forward trajectories. The PILT code was obtained after e-mail correspondence with Jerome D. Fast directly, but it should be available on a website in the near future.

The modifications naturally mean that changes made to FLEXPART between versions 6.2 and 8.2 not necessarily have been incorporated in PILT (or any other WRF compatible version of FLEXPART). On the other hand a lot of improvements have been made by Fast et al. For example, the FLEXPART-WRF and PILT models make use of more variables estimated by WRF instead of estimating them itself. These variables include U^*, surface heat flux and PBL height as well as turbulent kinetic energy. Since this application involves transportation on the sub-km scale we concluded that the PILT version was better, using as much as possible of the WRF calculated variables.

The work described in this thesis has been performed using PILT with some modifications:
- the emissions can now vary with time without having to follow a repeating daily/weekly pattern
- attempts to use the 3D cloud cover variables from WRF to derive 2D cloud cover used in regular FLEXPART-WRF

2.6 Instrumentation

During the field campaign different instruments were used for different applications. This section should be considered as a brief overview of the instruments and their use. For further details please refer to [1] and [15].

In addition to the instruments listed here, during the campaign measurements were also made using FTIR and Cospec instruments, but since data from those instruments have not been used for this study they are not described here.

2.6.1 Absorption spectroscopy and the DOAS principle

Each gaseous compound exhibit a unique absorption spectrum, i.e. a container filled with the gas will let different wavelengths of light (electromagnetic radiation) through to different extents, due to the molecular absorption of the incoming photons.

Absorption spectroscopy instruments are either *active*, containing their own light source (such as a lamp), or *passive*, using existing light in the environment (e.g. direct sunlight, scattered light from the sky, moonlight during the night, or infrared light from a hot surface).

In order to get gas composition information from an absorption measurement knowledge is usually required about the original spectrum emitted by the light source. In confined lab environments this is not a problem since emission spectra from the light source (such as a lamp) can be easily measured. For remote sensing applications though this is more difficult, since there are many different processes involved that change the wavelength composition of the light, including reflectance and Rayleigh scattering from water and atmospheric particles. However, fortunately, these processes do not cause any narrow signals in the wavelength spectrum. In Differential Optical Absorption Spectroscopy (DOAS), the collected spectra are high-pass filtered, removing these effects, leaving the (superimposed) characteristic spectra of molecules present in the gas mixture. In the wavelength region used in the instruments in this study (ultra violet, 305-325 nm) the compounds of concern are mainly SO_2 and O_3.

A short example is shown here. For light with an intensity I_0 going through a path length l containing gas with concentration c, from the Lambert Beer law we have the absorbance $A = -\log_{10}(I/I_0) = \sigma cl$, where the molecular cross section σ is a function of compound and wavelength. By studying the differences in absorption for two wavelengths close to each other with known cross sections we can calculate the concentration using

$$\log_{10}\frac{I(\lambda_1)}{I(\lambda_2)} = \log_{10}\frac{I_0(\lambda_1)\cdot 10^{-\sigma(\lambda_1)cl}}{I_0(\lambda_2)\cdot 10^{-\sigma(\lambda_2)cl}} = (\sigma(\lambda_2)-\sigma(\lambda_1))cl \tag{4}$$

In terms of the absorbance,

$$A_n = A(\lambda_n) = -\log_{10}\frac{I(\lambda_n)}{I_0(\lambda_n)} = \sigma(\lambda_n)cl$$

we can instead write (4) as

$$\log_{10}(10^{A_2-A_1}) = (\sigma_2-\sigma_1)cl$$

and retrieve the concentration c by

$$c = \frac{A_2-A_1}{l(\sigma_2-\sigma_1)}$$

This is of course generalised and automated for a whole range of wavelengths and not just two. Multiple chemical compounds can also be detected by superimposing solutions for their characteristic spectra.

2.6.2 Measuring strategy

The DOAS measurements on volcanic gas emission is made by pointing a telescope to the sky. The light is focused into a fibre which is connected to a spectrometer containing a grating which like a prism splits up the light into its different wavelength components onto a linear CCD array which registers the light intensity.

As seen in Lambert Beer's law above, the absorption unit is concentration times path length, meaning that it is not possible from an individual measurement to distinguish between a high concentration over a small path length and a low and widespread concentration. This is illustrated in fig. 9, where the two plumes A and B will give the same measured signal. Since the telescope is usually pointed to the sky the column is vertical and the measured number is called the vertical column density (with unit e.g. number of molecules per unit area). If the telescope is instead tilted with an angle α we instead have a slant column and the path length becomes a factor $1/\cos\alpha$ larger due to geometry. In fig. 9, scan 3 gives a vertical column but the others (1, 2, 4 and 5) give slant columns.

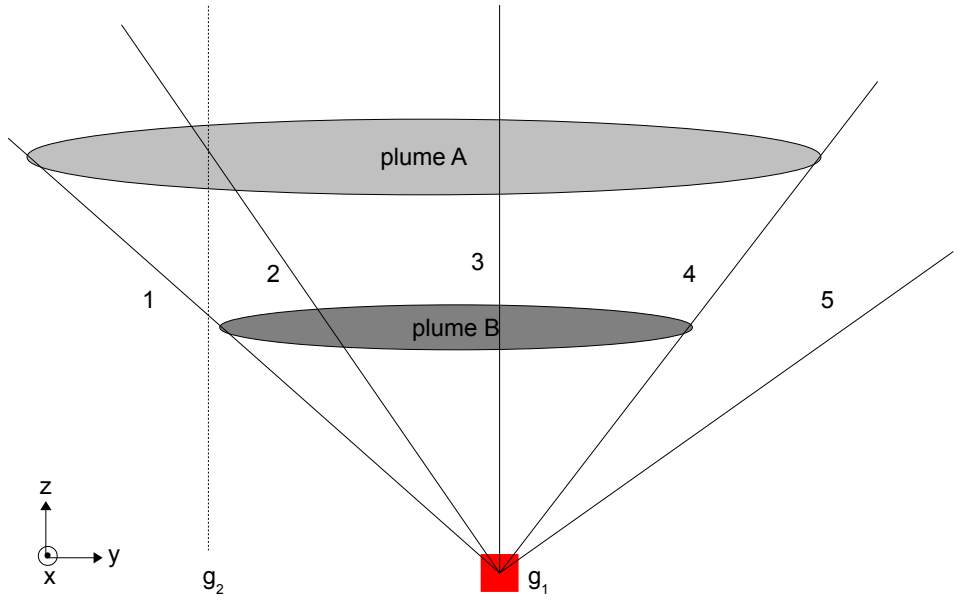

Figure 9: Sketch in a vertical plane depicting an instrument at ground position g_1 and two different plumes, A and B, above. The wind is blowing in the positive x direction, i.e. out from the paper.

The geometrical distribution of the volcanic plume is measured mainly in two ways. The first is by having a vertically pointing telescope mounted on a car driving under the plume as in fig. 10. Since the position of the car can be quite precisely determined (e.g. by GPS) the distribution of the plume is then known for the vertical columns right above the travelled path. Although this is a very straightforward method it is not very practical as it requires somebody to drive the full distance under the plume for every single measurement. It is therefore economically feasible only during field campaigns and not on a daily routine basis.

The second way is by using a stationary instrument that make sequential measurements in different angles, starting from one horizon, step by step scanning over the sky to the other horizon, e.g. as in fig. 9 for scans 1 through 5. By assuming a small vertical extent of the plume, the vertical columns for their respective ground position (e.g. g_2 for scan 2 in fig. 9) can then be approximated by multiplying by the cosine of the angle.

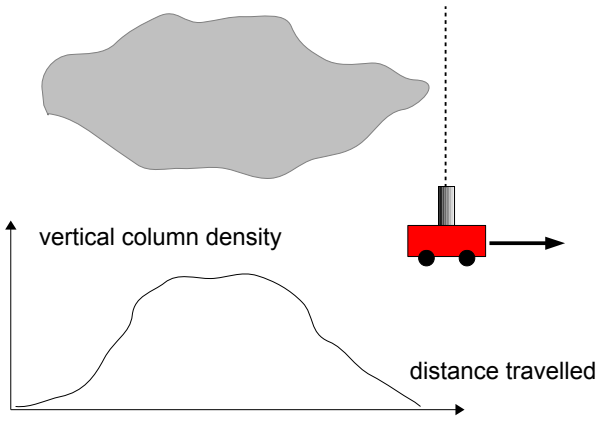

Figure 10: Mobile traverse. As the car travels under the plume the spectrometer detects the molecules right above it.

2.6.3 Flux measurements

The absorption measurement gives us the vertical column density, which has the unit molecules (or mass) per area. If a plume is passing over a measuring station as in fig. 9 and the vertical column densities are known as a function of distance from the station, one can integrate to obtain the area, which corresponds to the total molecules above that path and has unit molecules per meter. The total flux through the area can then be obtained by multiplying with the wind speed of the plume perpendicular to the path, so that mol/m times m/s yields mol/s. Since the flux is linearly dependent on wind speed it is of importance to have access to good quality wind data. Usually it is assumed that the wind speed in the plume is constant over the cross-section, and the value from just one altitude is used.

2.6.4 Plume speed and plume height

An approximation for the position of the plume centre can be obtained by locating the maximum value from two or more instruments by triangulation. However, often the conditions are not favorable for triangulation, e.g. when the plume can only be seen by one instrument. By time-correlating two simultaneous measurements made from the same telescope with a small angular difference ϕ the plume speed v and plume height H can be coupled as

$$\phi \approx \tan\phi = \frac{X}{H} = \frac{v \cdot \Delta t}{H} \tag{5}$$

where X is the relative distance between the two measurements and Δt is the time difference obtained after correlation. This is shown in fig. 11. If instead the instrument is moving and the plume is considered stationary (which is a valid assumption, since the traverse is made nearly perpendicular to the wind direction and the measurement time is short) we can determine the plume height. The disadvantage is of course then the labour involved with making a traverse, as mentioned in section 2.6.2. When neither triangulation nor traverses are available the release altitude (volcano summit) is used as plume height instead.

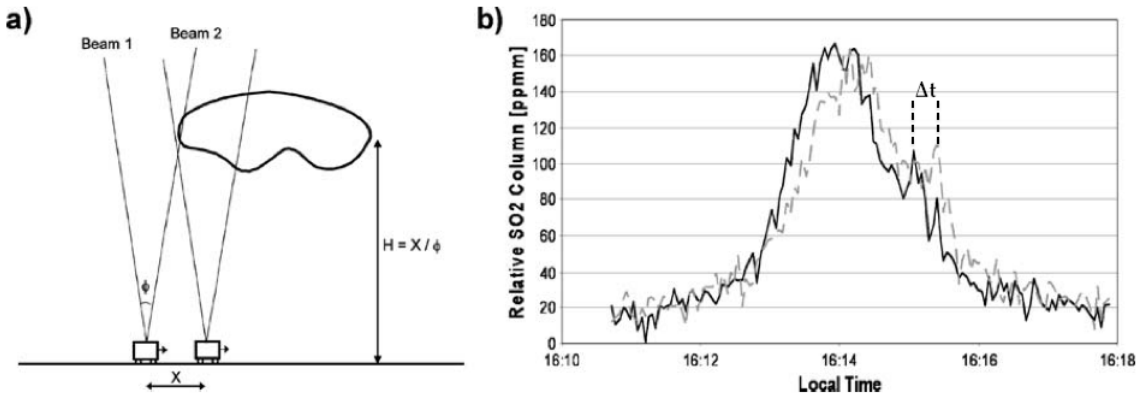

Figure 11: Left: Measurements with a dual-beam mini-DOAS at two different times separated by a relative distance X ($= v \cdot \Delta t$). By either traversing with the spectrometer below the plume or letting the plume pass over a stationary instrument either the plume height or speed can be calculated from the other using eq. (5). Right: An example of the time series from a dual-beam measurement with an approximate Δt marked in the figure. Both figures from [16].

2.6.5 The NOVAC instrument

Instruments developed in the DORSIVA project were fine-tuned and installed on many different sites from the start of the project in 2004. The instrument (version 1), which can be seen in fig. 12a, consists of a telescope, a prism, a rotating hood, an optical fibre, a spectrometer, a radio modem, a GPS receiver and a temperature sensor, all controlled by an embedded PC and support electronics and powered by solar panels.

For the version one instrument, two different scanning patterns are available, one flat and one conical with 60° cone angle as shown in fig. 12b. The main advantage with the conical is that it enables full cover around a volcano using fewer instruments.

Details can be found in [1] and [15].

2.6.6 Mobile mini-DOAS

The mobile mini-DOAS consists of a telescope, an optical fibre and a spectrometer. The spectrometer is connected directly to an ordinary laptop computer via USB cable. The hardware is similar to what is used in the NOVAC instrument with the same spectrometer and telescope. The rest is simpler, since the connected laptop computer handles both spectrometer controlling, data processing and storage as well as supplying power over the USB interface. Since the telescope is mounted firmly and only measures to the zenith there is no motor needed for changing scanning angle as in the NOVAC instruments.

With the telescope mounted on a vehicle such as a car, boat or even an aircraft, the traverse gives information on vertical column density above the travelled path as in fig. 10.

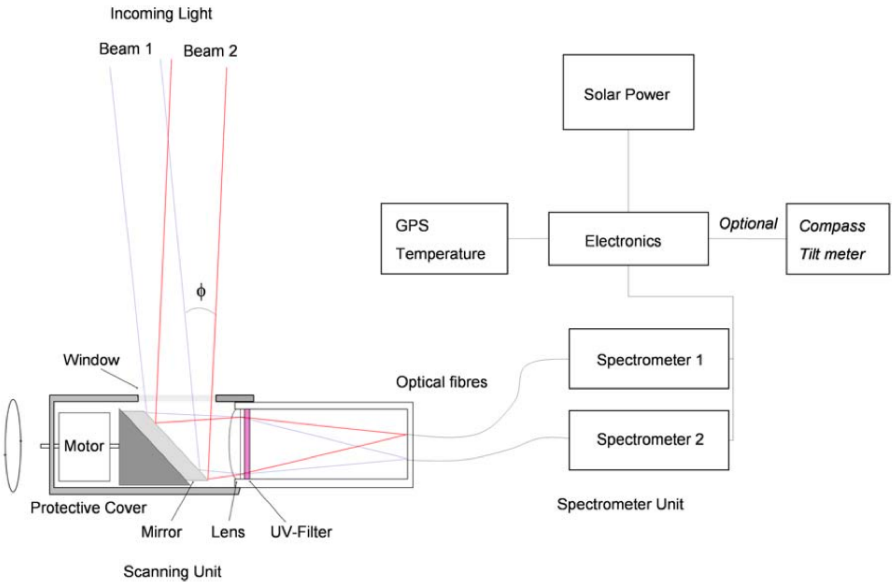

(a) Schematic view of the NOVAC instrument. From [1].

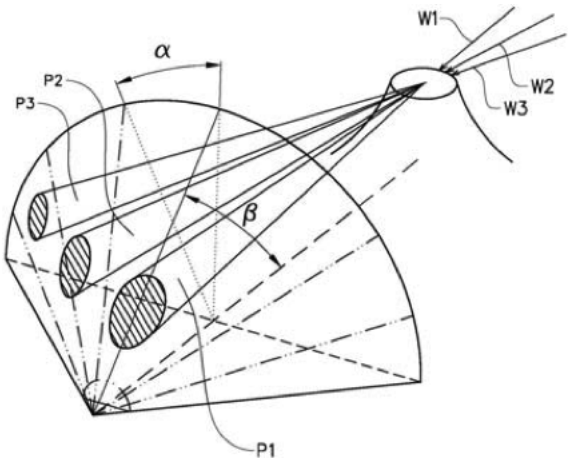

(b) Conical scanning pattern. From [1].

Figure 12: The NOVAC instrument, version 1.

2.6.7 Rapid deployment system

This system consists of three scanning instruments similar to the NOVAC instruments. One instrument is shown in fig. 13a. As the name implies it is designed for rapid deployment when an eruption is approaching or even ongoing. The stations should then be installed in such geometry to cover a relevant area around the volcano. The telescope is mounted to a tripod and the electronics, such as spectrometer, embedded computer, modem, power supply and voltage regulator, are mounted and inside a hard plastic case for a limited protection against the environment. The solar panels used (UnatSolar 60W) are foldable and very light for easy transportation. Compared to the NOVAC instruments, this system has improved communication (fig. 13b) by first utilising radio modems (Freewave 2.4 GHz) to transmit the data to a single computer which quickly processes the data from the three scanners and then sends it to a server using a satellite modem (SABRE I, utilising the BGAN network which provides coverage using the I-4 geostationary satellites). Just like a set of NOVAC instruments, the data from the rapid deployment system can provide measurements of emission, wind speed, plume height and plume concentration profiles (tomographic measurement).

(a) One of the instruments with electronics box and solar cells.

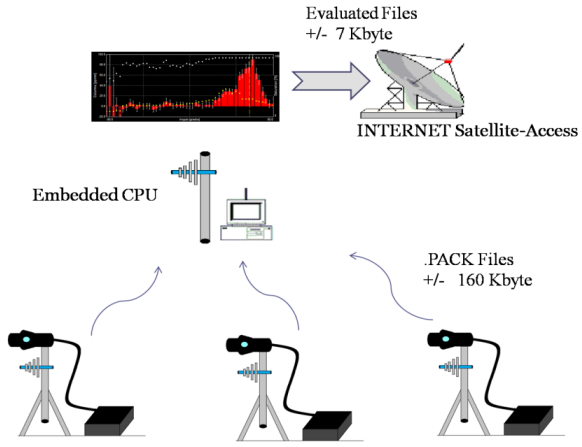

(b) The communications path in the Rapid Deployment System.

Figure 13: The Rapid Deployment System. Both pictures from [17].

3 Method

The work was carried out in three major parts: 1. Field work on Popocatépetl volcano. 2. Implementing FLEXPART-WRF/PILT on the volcanoes. 3. Validation of the model using measurements from field campaign and NOVAC instruments.

3.1 Field campaign on Popocatépetl, Mexico

Within the project FIEL-VOLCAN run by Universidad Nacional Autónoma de México (UNAM), Mexico City, in April 2010 a three week campaign was taking place around Popocatépetl volcano. Stationary and mobile measurements were conducted by researchers from UNAM and CENAPRED, Mexico City as well as from universities in Heidelberg, Palermo and Gothenburg.

A typical (and ideal) measurement day started by checking meteorological forecasts, both publicly available regional as well as self-made local from WRF. From the wind data, an estimate of the plume direction was made and the teams set out in cars, making traverses retrieving the vertical columns. When the plume centre was found, the stationary instruments were deployed at strategic places on both sides of the plume, preferably equidistant from the crater, while the mobile continued traversing back and forth.

In reality of course it was more difficult, as changing weather and wind directions made it hard to get as much data as preferred. The road infrastructure was very diverse, ranging from straight highway of high standards to extremely rocky, curvy, steep paths through jungle-like areas. Some kilometres of the roads were also under construction work during the campaign period, causing stops and delays when the plume was heading in that direction. Also, it was not always easy to find places to put down the instruments from where there was both clear view of enough of the horizons at the same time as safe and easy to reach. Permission was usually asked from and granted by the local mayor, but in some cases the responses were negative. In the end, from about one effective week of measurements the number of good traverses per instrument is below ten.

3.2 Running the dispersion model

As seen in the workflow in fig. 7, the method involves many different steps, which also all contain different data structures which have to be properly interfaced to work together. The FLEXPART-WRF/PILT model uses meteorological input data from WRF, so first this data was produced for the time interval and location of interest. Then FLEXPART-WRF/PILT was setup and the output was processed and compared with data from measurements.

3.2.1 Weather input data generation

The WRF data was produced using a setup provided by Patrik Norman with WRF model 3.2.1 using ECMWF analysis datasets. The WRF model was run on the Beda cluster at Chalmers, using 16 nodes with 8 cores each consuming about 45 minutes real time (96 core-hours) per 24h data. Three nested grid domains were used, with resolutions 9, 3 and 1 km, each 91x91x43 points and centred on the volcano as in e.g. fig. 8.

No validation of the WRF data was made directly. The WRF model in itself has been validated against measurements in numerous articles. More validation may be needed however in the tropics (where many of our volcanoes are located) since the immense heat flux causes large convection, but since this is out of the scope of this work and since there are also many people running the model in those regions we will skip that for now.

3.2.2 Setting up FLEXPART-WRF/PILT

The dispersion model was run separated as one simulation per day, for parallelisation and to avoid possible errors or inaccurate meteorological data for a short time to hang on for longer periods. Since it takes a while after the start of an emission to form a complete plume, each run was started at 22:00 UTC on the day before and ending on 00:00 UTC the day after. However, since the measurement stations used in this work are located in Latin America and Africa and rely on daylight there will be no measurements to compare with for the early hours (UTC). The emission over time was set to constant to make comparison between different times easier and to avoid dependence on flux measurement error and availability.

For each output time interval the model produces two different sets of tab-separated text files: partposit and gridconc. The partposit files contain the position of individual particles at each output time. The gridconc files contain the concentrations in the grid cells specified by the output grid which is just the sum of all particles within a user-defined grid, which in this case is 91-by-91-by-32 levels with horizontal resolution of about 1 km. The vertical size of the boxes increase with increasing altitude.

3.3 Implementing the dispersion model for comparison with DOAS instruments

In order to compare the dispersion data with measurements, a number of different routines were implemented in MATLAB. In a first simple approach to compare with the mobile traverses, two-dimensional vertical slices were made through the concentration grid data. The weighted average position of the highest concentrations from the measurement was taken as midpoint for a 25 km slice perpendicular to the volcano and then for a number of equally spaced points along this slice the vertical columns were summed up.

To compare with a NOVAC instrument, a scanning was simulated through the gridded data from the location of the instrument. Due to fluctuations in wind directions, another scanning was also made from the point directly below the highest FLEXPART concentrations.

To quantify the comparison, the following simple measures were used. First, instrument *angular coverage* of the plume was determined, with an example of the half-intensity angles shown in fig. 14. The *plume height* can be directly measured when the plume is seen by two or more instruments by triangulation, and also can be quite easily calculated from the model, making it a good parameter for validation. Knowing the angular coverage together with the plume height (either from triangulation measurement or from FLEXPART) we could also derive the *full width at half maximum* by adding the parts of the plume on the left and right side

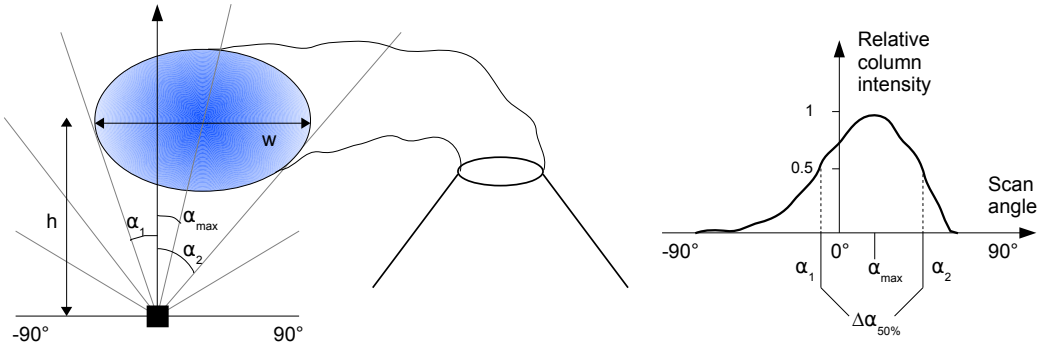

Figure 14: A plume passing over a scanning instrument (with wind direction out of the paper towards the reader) will give a vertical column distribution as shown in the right graph. From this the angular coverage for the half-intensity was calculated. By multiplying the tangent of the angles with the plume height the full width at half maximum is retrieved.

of zenith, giving (taking into account the signs of the angles)

$$\text{fwhm} \approx h \cdot (\tan \alpha_2 - \tan \alpha_1)$$

where h is the plume height and α are the angles of the first and last angles above half max intensity as in fig. 14.

However, as the plume width increases with the tangent of the angle, for high angles a small error in angle will amount to a large error in the calculated plume width. Measurements were therefore selected on the basis of the angle of the highest slant column density being within a certain angle from the zenith directly above the instrument, as well as setting a criterion for the maximum width of the plume by constraining the half maximum angles α_1 and α_2 to be within $\pm 45°$.

3.4 Implementing the model for SO_2 ground dose

One reason for implementing the dispersion model on Nyiragongo was to assist the SIDA project as mentioned in section 1.1.2. Therefore, in addition to the routines already made for the comparison of dispersion data with instrument data at Popocatépetl, automation routines were also made to process simulations over longer time periods. The dispersion model was operated as individual runs for each day for a number of consecutive days, producing output for every hour. The hourly concentrations on the grid were added and stored as single file for the period.

Initially, attempts were made to implement wet deposition, but since the handling of cloud cover are significantly different between ECMWF and WRF it ultimately failed and will have to be assessed later. Finally, the total doses during a period were calculated for the lowest three model height levels, 0-66 m above ground level.

4 Results

The following pictures show concentrations on a selection of times chosen based on quality of available measurements.

Another main result which is not directly shown below is the amount of code and routines produced which make it easy to produce more dispersion simulations and comparisons with measurements for any time and location with available meteorology data.

4.1 Vertical SO_2 columns compared with traverse data

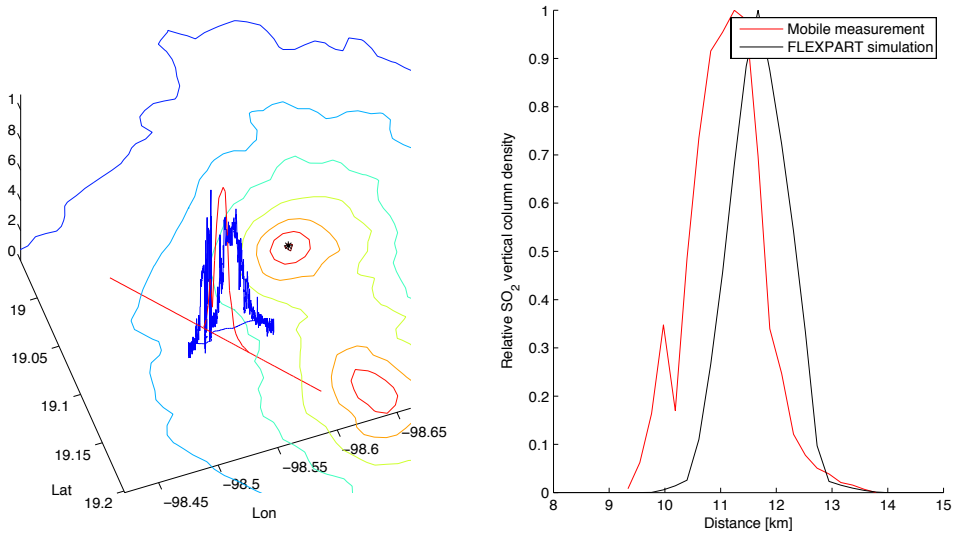

Figure 15: Mobile measurement (car traverse on 2010-04-24 at 16:38 UTC) compared with concentrations from FLEXPART dispersion simulation. The coloured lines in the left figure are the topographic contours with the volcano summit marked as the black dot. The red straight line marks the plane perpendicular to the volcano which gives the projection of the measurement as the red curve. The right figure shows the same projection of the measurement compared with the corresponding values from FLEXPART.

Fig. 15 shows an example of a vertical slice through the modelled data. The plume was measured by car travelling on the road marked by the bottom solid blue line giving the vertical columns above it. Out of 6 traverses with good measurement data from the Popocatépetl campaign, 4 showed good agreement similar to this one, while one had large deviation in wind direction from WRF and one underestimated the plume width by about half.

4.2 Model data compared with scanning instruments

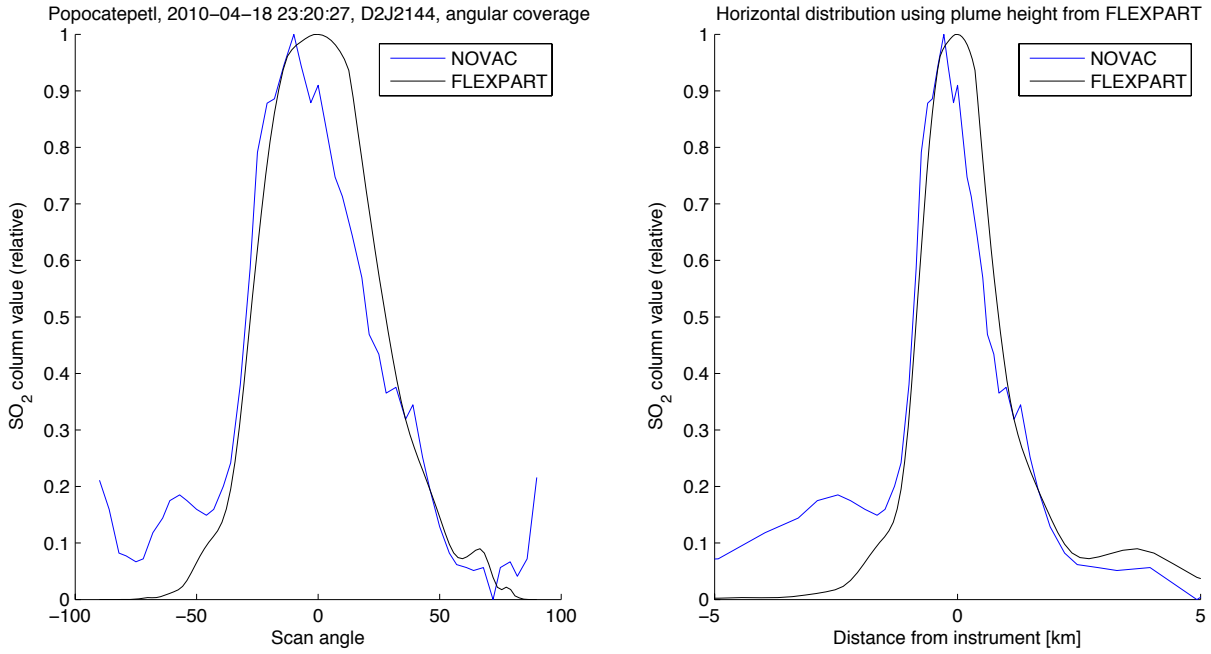

Figure 16: The left image shows a simulated scan in the FLEXPART data (black) compared with measurement from a scanning instrument (blue). In the right image the same data is shown but with distance from instrument position on the x axis instead of angle, calculated using plume height from FLEXPART.

In fig. 16 an example of a simulated scan is shown. From this data, the full width at half maximum was calculated, provided plume height data is available. The plume angular coverage is shown for Popocatépetl and Nyiragongo in fig. 17a and the calculated full width at half maximum for the plume for the same data in fig. 17b. Due to the different placement of instruments at the different volcanoes, among these three volcanoes, only Tungurahua delivers triangulations often enough to be reliably used for plume height. For Popocatépetl and Nyiragongo, the plume height from FLEXPART was used instead, giving the plots seen in fig. 17b.

Out of 3358 measurements made by the instruments at Tungurahua between January 2nd and 23rd 2010, about 300 fulfilled the criteria that the plume centre should be within ±10 degrees from zenith above the instrument and the half maximum values should be within ±45 as well as having an estimated plume height error of less than 30%. The angular coverage of the plume for these measurements are shown in fig. 18a and the plume full width at half maximum in fig. 18b.

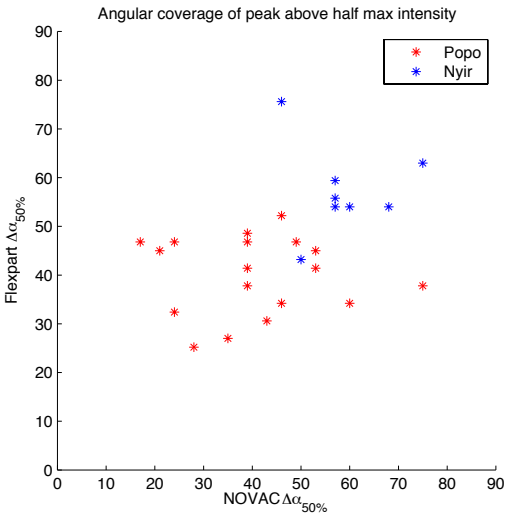

(a) Angular coverage.

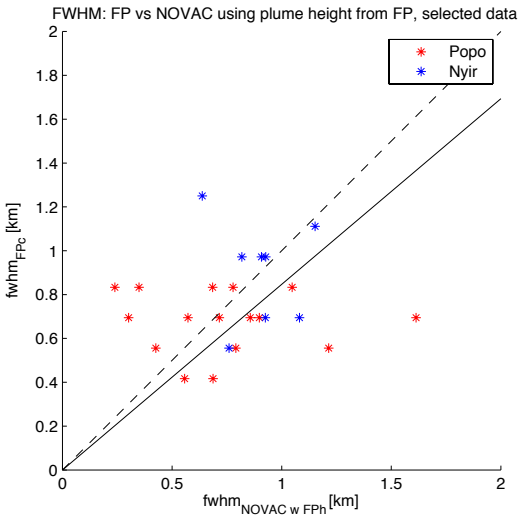

(b) Full width at half maximum using plume height from FLEXPART.

Figure 17: Data from 26 scans at Popocatépetl and Nyiragongo. The trend in the right figure has a slope of 0.84.

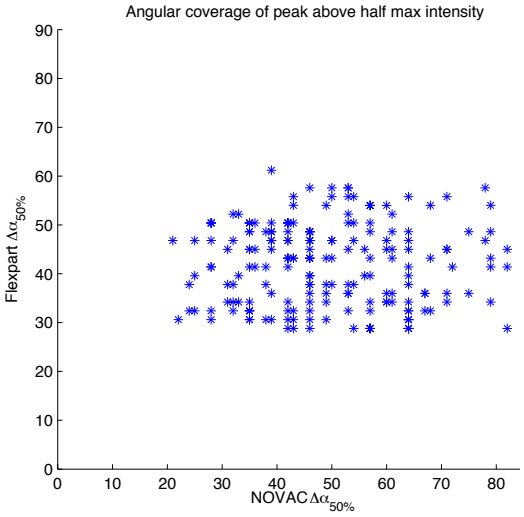

(a) Angular coverage.

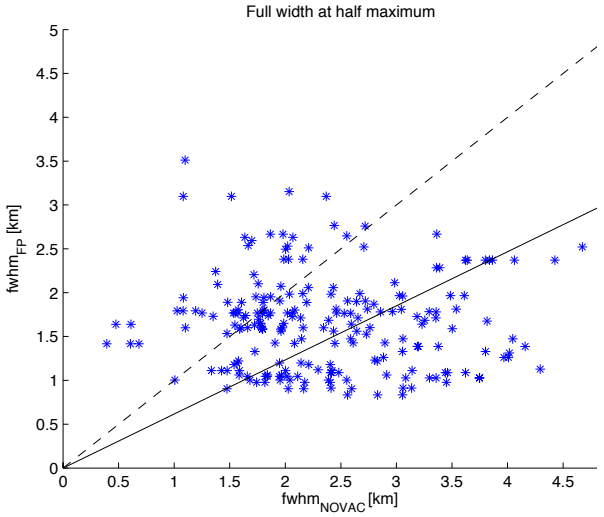

(b) Full width at half maximum using triangulated plume height.

Figure 18: Data from 300 scans at Tungurahua using plume height from triangulation. The trend in the right figure has a slope of 0.596, although that measure is questionable for a spread as large as this.

A comparison between the simulated plume height from FLEXPART-WRF/PILT and these 300 measurements is shown in fig. 19a.

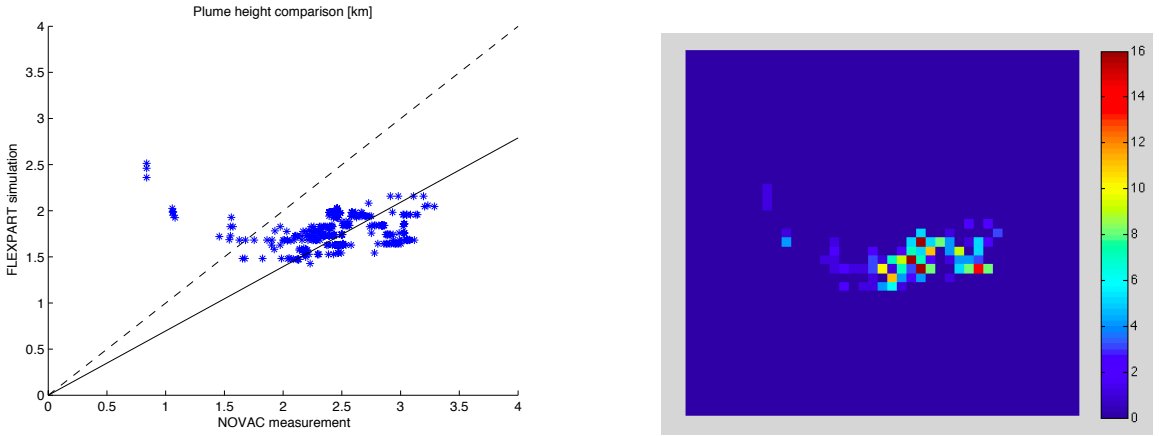

(a) Scatter plot and trend line.

(b) Density representation of the same data. The colors indicate number of samples.

Figure 19: Plume height from FLEXPART simulation plotted against measurement by NOVAC instrument by triangulation. The trend (solid line) in the left figure has a slope of 0.6975.

4.3 Ground dose of SO_2 at Nyiragongo

Dispersion simulations were run for all of December 2009 and the concentration fields for all independent hours were added. The sum of the lowest three vertical levels (corresponding to about 0-66 m above ground level) can be seen in fig. 20. The values are proportional to total emission times the exposure time of the respective ground area.

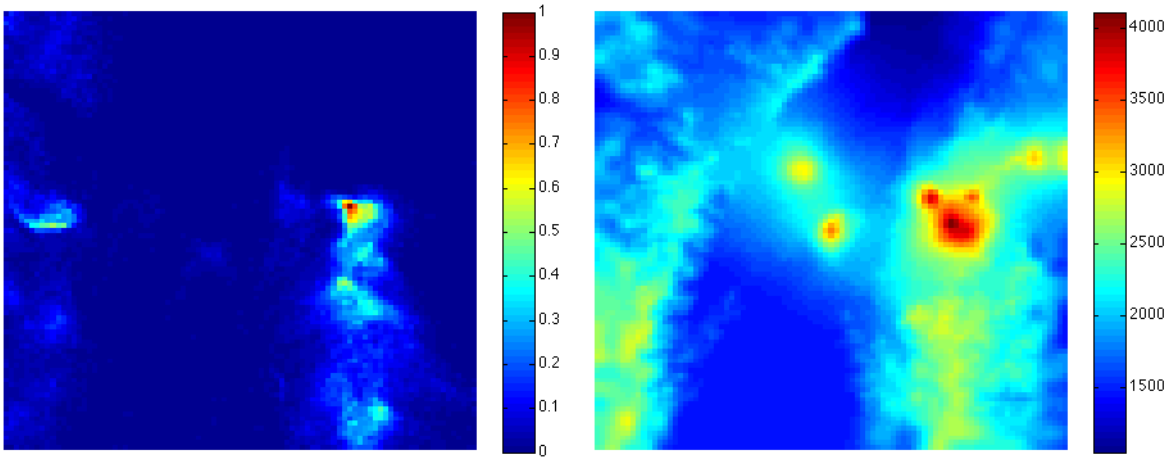

(a) SO_2 dose. (b) Topography.

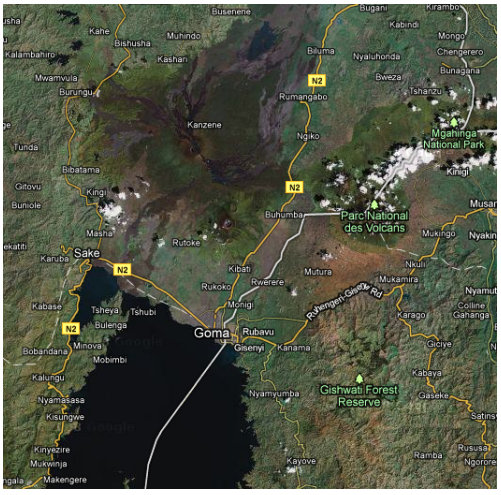

(c) Map. ©2011 Google, Tracks4Africa

Figure 20: Average dose of SO_2 (conc·time) for the sum of the three lowest model z-levels, corresponding to 0-66 metres. In figures (b) and (c) the topography and map over the same area are shown for comparison. The total coverage of the maps are about 80 by 80 km.

5 Discussion

For the particular simulated scan shown in fig. 16, the difference in simulated wind direction makes the plume appear a little too far to the right in the model. The plume width in the simulation is close to the measured, but the fine structures in the measurement can of course not be seen in the model.

In fig. 17a there is a strong tendency of separation between measurements from the two volcanoes. This is expected, as plumes emitted from Popocatépetl will be less dispersed than plumes from Nyiragongo when measuring from approximately the same distance. This is largely due to their different summit altitudes, since winds speeds are higher at higher altitudes.

The many measurements from Tungurahua in fig. 18b show a clear stratification in the plume heights. This shows that the dispersion model only contains a discrete number of different plume widths. That could be explained by the spatial resolution of the output grid, but also by the dependence on the time resolution in the output from FLEXPART, since multiple measurements are compared to the same simulation data.

The plume height in fig. 19a show a dependence between measurement and simulation, although the model seems to underestimate the plume by 30%. Unfortunately, this is only using data from one volcano, so it may be too early to draw any general conclusions for conditions with different winds or topography.

For the SO_2 dose in fig. 20, when comparing with the topography we see that the doses naturally are higher on mountain peaks (where the plume has swept over more frequently) than on the flatlands in between. Some other locations show stronger dose than others due to being more often downwind from the volcano. Similar dosage maps can later be compared with data from chemical diffusion samplers.

Since the dispersion modelling is heavily dependent on the meteorological input any improvement in that data will also improve end results from the dispersion model. Therefore it is not clear whether discrepancies between measurements and modelled data is due to the dispersion model or bad weather data.

Previous preliminary results by the group indicate that the wind speed is more accurate than the wind direction. A countermeasure for this has been made in the comparison with the scanning instruments by only selecting data where the plume direction is within ± 10 compass degrees from the scanning instrument.

The low time resolution of the data from ECMWF (6 hours) means that we cannot fully resolve events such as frontal passages (where the conditions are changing very rapidly) and other phenomenon occurring quickly. Even if the global model predicts a weather front to pass somewhere in between these two times it may not be able to correctly predict at what time within more than a few hours.

A quantifiable number indicating the quality of the wind data would be preferable but is not easily determined without further wind measurements available.

Under good conditions, the instruments may deliver data as often as every five minutes. This high time resolution of the instrumental data is not matched by the output intervals from the model. A brief investigation showed no major improvements using output every 15 minutes, although the same hourly WRF data as input. Due to disk space usage and convenience, it was finally chosen to store model output just every hour. The results may of course still improve using higher time resolution from the ECMWF or WRF data.

Further on, vegetation is not directly taken care of in the model, so near-ground

concentrations should be evaluated carefully and could be more variable than they seem. This is partly counteracted by land use factors incorporating the surface roughness, but such data is rather low resolution. No sampler measurement are available to compare with so the dose results should be more viewed as a proof of concept for possible uses of the dispersion model data products.

An approximation made but not yet discussed is that this implementation of the dispersion model treats SO_2 as an inert gas. This may not be such bad approximation though since the distance from the point of measurement to the crater is quite small compared to long-range transport. The lifetime of SO_2 in the atmosphere is about 4 days (from [18]), meaning it will have time to be transported thousands of kilometres under normal atmospheric wind conditions.

These and many similar approximations are due to the fact that the model is more often used for medium to long-range transport than in this few kilometre setting.

5.1 Suggestions for future work

Given more time, it would be interesting to compare the results with other models, for example HYSPLIT and EMEP but also FLEXPART 8.2 using ECMWF data (non-WRF). For the SIDA project the deposition (dry as well as wet) is important and not really assessed here so far. From an environmental impact point of view it would also be important to sooner or later implement atmospheric chemistry as well as wet chemistry.

6 Final words

FLEXPART-WRF/PILT works quite well for applications to volcanic gas emissions even for this small-scale transport of just tens of kilometres or below. The traverse measurements show good agreement in about two thirds of the cases. For easily quantifiable parameters such as plume height, angular coverage and plume width, the model gives a large spread, which leads to the conclusion that the model works best as a hint in the right direction, maybe more for qualitative results than for quantitative so far. Improvements in input weather data would most likely improve the results considerably, although it is unclear exactly how much of the observed spread is due to bad weather data and how much to e.g. FLEXPART-WRF/PILT itself being written for more long-range transport scenarios.

References

[1] Galle, B., M. Johansson, C. Rivera, Y. Zhang, M. Kihlman, C. Kern, T. Lehmann, U. Platt, S. Arellano, and S. Hidalgo (2010), *Network for Observation of Volcanic and Atmospheric Change (NOVAC)—A global network for volcanic gas monitoring: Network layout and instrument description*, J. Geophys. Res., 115, D05304, doi:10.1029/2009JD011823

[2] *Popocatépetl, eruptive history*, Global Vulcanism Program, Smithsonian Institution, `http://www.volcano.si.edu/world/volcano.cfm?vnum=1401-09=&volpage=erupt`

[3] Rivera, C. (2009): *Application of Passive DOAS using Scattered Sunlight for quantification of gas emissions from anthropogenic and volcanic sources*, PhD thesis, Chalmers university of technology

[4] *National emissions reported to the Convention on Long-range Transboundary Air Pollution (LRTAP Convention)*, Annual European Union LRTAP Convention emission inventory report 1990-2008, European Environment Agency. Link to data viewer: `http://dataservice.eea.europa.eu/PivotApp/pivot.aspx?pivotid=478`

[5] Bosanquet, C.H., Pearson, J.L. (1936) *The spread of smoke and gases from chimney*, Trans. Faraday Soc., 32:1249.

[6] Beychok, M.R. (2005) *Fundamentals of Stack Gas Dispersion*, 4th ed., self-published, `http://www.air-dispersion.com/`

[7] Wikipedia: *Air pollution dispersion terminology: Characterization of atmospheric turbulence: The Pasquill atmospheric stability classes*, `http://en.wikipedia.org/wiki/Air_pollution_dispersion_terminology#The_Pasquill_atmospheric_stability_classes`, retrieved 2011-05-27

[8] *ERA-40*, ECMWF `http://www.ecmwf.int/research/era/do/get/era-40`

[9] The Weather Research and Forecast Model Website `http://www.wrf-model.org`

[10] Stohl, A., C. Forster, A. Frank, P. Seibert, G. Wotawa (2005): *Technical Note : The Lagrangian particle dispersion model FLEXPART version 6.2*. Atmos. Chem. Phys. 5, 2461-2474.

[11] *Development of a Lagrangian Particle Dispersion Model Compatible with the Weather Research and Forecasting (WRF) Model – Phase 1*, draft, Jerome D. Fast and Richard C. Easter, Pacific Northwest National Laboratory, 16 February 2006 (from e-mail correspondence)

[12] *Development of a Lagrangian Particle Dispersion Model Compatible with the Weather Research and Forecasting (WRF) Model – Phase 2*, draft, Jerome D. Fast and Richard C. Easter, Pacific Northwest National Laboratory, 19 October 2006 (from e-mail correspondence)

[13] *Development of a Lagrangian Particle Dispersion Model Compatible with the Weather Research and Forecasting (WRF) Model – Phase 3*, draft, Jerome D. Fast and Weiguo Wang, Pacific Northwest National Laboratory, 31 January 2007 (from e-mail correspondence)

[14] *The Lagrangian particle dispersion model FLEXPART, version 8.2*, A. Stohl[1], H. Sodemann[1], S. Eckhardt[1], A. Frank[2], P. Seibert[2], and G. Wotawa[3], 1. Norwegian Institute of Air Research, Kjeller, Norway, 2. Institute of Meteorology, University of Natural Resources and Applied Life Sciences, Vienna, Austria, 3. Preparatory Commission for the Comprehensive Nuclear Test Ban Treaty Organization, Vienna, Austria

[15] Johansson, M. (2009): *Application of Passive DOAS for Studies of Megacity Air Pollution and Volcanic Gas Emissions*, PhD thesis, Chalmers university of technology

[16] Johansson, M., Galle, B., Zhang, Y., Rivera, C., Chen, D., Wyser, K., *The dual-beam mini-DOAS technique—measurements of volcanic gas emission, plume height and plume speed with a single instrument*, Bull Volcanol (2009) 71:747–751 DOI 10.1007/s00445-008-0260-8

[17] Conde, V. (to be published 2011): *Development and Implementation of a rapid deployment system for monitoring volcanic gas emissions*, MSc thesis, Chalmers university of technology

[18] U. Platt, J. Stutz (2008) *Differential Optical Absorption Spectroscopy - Principles and Applications*, Springer